

Cite this: DOI: 10.1039/c1sm05470h

www.rsc.org/softmatter

PAPER

## Effects of crystalline subunit size on silk fiber mechanics†

Murat Cetinkaya,<sup>\*a</sup> Senbo Xiao<sup>b</sup> and Frauke Gräter<sup>\*cd</sup>

Received 17th March 2011, Accepted 9th June 2011

DOI: 10.1039/c1sm05470h

Here, we utilize a computational bottom-up approach to decipher the size effects of poly(alanine) crystalline subunits as they occur in most spider silks on silk fiber mechanics. We vary the crystal size in terms of their cross-sectional area, *i.e.* the number of layers of  $\beta$ -strands,  $S$ , in the crystal and the backbone length along the fiber axis,  $N$ . Meanwhile, other major parameters such as chemical composition, fiber crystallinity, and the relative orientation of the crystals in the fiber are constrained. The computational approach incorporates Molecular Dynamics and Finite Element simulations of the crystalline subunits along with Finite Element simulations of a two phase silk fiber model in order to determine the stress–strain behavior, elastic moduli and toughness properties. Overall, the fiber elastic modulus and toughness increase with the length of the crystals as given by the number of residues in the  $\beta$ -strands ( $N$ ), and decrease with the crystal cross-section area, *i.e.* the number of  $\beta$ -strands per crystal ( $S$ ). The smallest cross-sectional area investigated, a  $3 \times 3$  crystal ( $\sim 1 \text{ nm}^2$ ), shows the highest sensitivity of the mechanical properties towards the crystal length. The presented approach is a versatile tool in artificial fiber design since it does not require any empirical parameters and it is similarly applicable to other semicrystalline polymeric systems or composite materials.

## Introduction

There has been a long-standing and growing interest in natural silk fibers due to their intriguing mechanical properties. Mimicking the mechanical properties of these biological materials has remained a challenge due to their structural complexity. Silk fibers are assemblies of micron length fibrils that are composed of two main constituents, namely the crystalline and amorphous subunits (Fig. 1a). Crystalline subunits are assemblies of poly(alanine) or poly (GA)  $\beta$ -strands staying intact *via* hydrogen bonds and side chain interactions. Amorphous subunits are bundles of disordered peptide chains filling up the remaining fibrillar volume. Through a hierarchical arrangement of the strong crystalline and elastic amorphous subunits at the atomistic scale, silk fibers exhibit superior mechanical properties such as high toughness, elasticity, and rupture strength.<sup>1,2</sup> These properties can be further fine-tuned by the amino acid sequences

of the constituent proteins<sup>1,3–5</sup> and the conditions during fiber formation.<sup>6–9</sup> For instance, the reeling speed of spider silk fibers and their interaction with water affect the size of the crystalline subunits,<sup>7</sup> and the pretension (*i.e.* initial extension) of the disordered peptide chains in the amorphous subunits,<sup>9</sup>

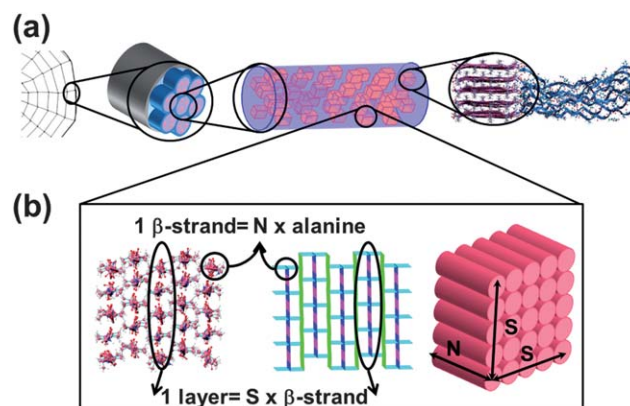


**Fig. 1** The structural hierarchy in spider silk fibers. (a) Fibers of spider dragline silk are composed of fibrils which are made up of strong crystalline subunits (pink) segregated in a soft amorphous matrix (blue). Crystalline subunits are assemblies of  $\beta$ -strands, while the amorphous subunits are bundles of disordered peptide chains. (b) The crystalline subunits (left: all-atom model, middle: skeleton model) are composed of layers containing poly(alanine)  $\beta$ -strands with their backbone axis oriented along the fiber axis. The size of the crystalline subunits is quantified by the number of  $\beta$ -strands in one layer,  $S$ , and the backbone length (*i.e.* the number of alanines in a  $\beta$ -strand),  $N$ .

<sup>a</sup>BASF SE, Carl-Bosch Strasse 38, Ludwigshafen, 67056, Germany. E-mail: murat.cetinkaya@basf.com; Tel: +49 621 6041702

<sup>b</sup>Heidelberg Institute for Theoretical Studies, Schloss-Wolfsbrunnengasse 35, Heidelberg, 69118, Germany. E-mail: senbo.xiao@h-its.org

<sup>c</sup>Heidelberg Institute for Theoretical Studies, Schloss-Wolfsbrunnengasse 35, Heidelberg, 69118, Germany. E-mail: frauke.graeter@h-its.org; Fax: +49 6221 533298; Tel: +49 6221 533267

<sup>d</sup>CAS-MPG Partner Institute and Key Laboratory for Computational Biology, Shanghai Institutes for Biological Sciences, Chinese Academy of Sciences, Yueyang Road 320, Shanghai 200031, P.R. China.

† Electronic supplementary information (ESI) available: The text includes the supporting figures showing the complementary elasticity and rupture properties of the crystalline subunits with different sizes. See DOI: 10.1039/c1sm05470h

respectively. Experimental studies on silk fibers have provided great detail about their chemical and physical nature such as the mechanical response at the atomistic and macroscopic levels,<sup>1,3,7–11</sup> the crucial features of the silk protein sequences,<sup>4,5,12</sup> and the size and architecture of the building blocks.<sup>7,9,13–16</sup> There has also been considerable effort regarding the artificial synthesis of spider silk fibers.<sup>6</sup>

Due to technical limitations in the experimental studies, computational methods have been the method of choice for understanding the relationship between the subunit size and macroscopic fiber properties. Many computational studies at discrete length scales aimed at understanding the mechanical characteristics of the individual building blocks at the atomistic level<sup>17–19</sup> and the macroscopic properties of the spider webs as an assembly.<sup>11,20,21</sup> The size effect of the building blocks has been a recent point of interest<sup>22,23</sup> as it is a requisite for designing artificial silk fibers with tailored mechanical properties. Among other methods in the literature,<sup>11,18–22</sup> the bottom-up computational approach that we have recently developed takes the atomistic properties of silk building blocks into account. Without any empirical parameters it enables one to investigate the macroscopic fiber properties *via* continuum scale models.<sup>24</sup> With this approach, one is not limited to Molecular Dynamics simulations but is able to build continuum scale models that allow a tremendous decrease in the required computational power ( $\sim 6$  orders of magnitude). By scanning through certain design parameters (*e.g.* crystallinity, structural architecture, *etc.*), our recent investigations showed that silk crystals are the source of strength in silk fibers while they stay intact as the cross-linking sites between disordered peptide chains that provide elasticity for the silk fibers. The structural arrangement of the silk building blocks was also found to have a profound effect on the silk fiber toughness.

In this study, we investigate the significance of another major design parameter for silk fiber mechanics, the size of the crystalline subunits, by utilizing our bottom-up computational approach that bridges atomistic Molecular Dynamics (MD) and continuum scale Finite Element (FE) calculations.<sup>24</sup> First, the effects of the crystal length and the cross-sectional area on crystal elasticity and toughness as obtained from MD simulations are presented. The optimum size for a crystalline subunit is discussed. On this basis, the relationship between the size of the crystalline subunits and the fiber mechanical properties such as elastic modulus, rupture strength and stress, and toughness are analyzed with FE models.

In this particular analysis, we focus on poly(alanine) silk crystals, but they share a similar structural architecture with poly(GA) crystals. Therefore, our findings are expected to be applicable for both crystal types. We utilize a random distribution of crystalline subunits in the fiber and include the effects of both tensile and shear loading on the crystals through a new pulling setup. The results from our comprehensive fiber model are in good agreement with previous experiments and they provide a framework in artificial fiber design.

## Materials and methods

Spider silk fibers are built of fibrils composed of highly ordered crystalline subunits being surrounded by the amorphous

subunits which are made of semi-extended, disordered peptide chains (Fig. 1a). As in our previous study,<sup>24</sup> we consider the crystalline and amorphous subunits of the spider silk fiber from the major ampullate gland of *Araneus diadematus*.<sup>1</sup> The crystalline subunit is composed of layers of  $\beta$ -strands from poly(alanine) peptides. The size of the crystalline subunits is expressed in terms of the backbone length (*i.e.* number of residues),  $N$ , and the number of layers,  $S$ , that is proportional to the cross-sectional area of the crystals (Fig. 1b). Therefore, the crystalline subunits are composed of  $S \times S$   $\beta$ -strands each of which is made up of  $N$  amino acids (*i.e.*  $S \times S \times N$  amino acids in a crystal).

## Molecular dynamics (MD) simulations

All MD simulations were performed with Gromacs 4.0.5.<sup>25</sup> The parameters for equilibrating the simulation systems were assigned the same as in our previous studies.<sup>17,24</sup> In summary, the OPLS-AA force field<sup>26</sup> for the peptides and the TIP4P model<sup>27</sup> for water were used. A time step of 2 fs was chosen, and simulations were performed at constant temperature (300 K) and pressure (1 bar), with periodic boundary conditions and with Particle-Mesh Ewald summations for long-range ( $>1$  nm) electrostatics.<sup>28</sup>

The all-atom models of the crystalline subunits were composed of anti-parallel  $\beta$ -strands of alanine. A simulation box with a  $\sim 3 \times 2.5 \times 2.5$  nm<sup>3</sup> crystal had  $\sim 35\,000$  particles including solvent molecules. The boundary conditions on the crystals were not restricted and the crystals stayed intact until the rupture point in MD simulations. Tensile stretching of the crystals was accomplished by symmetrically pulling the  $\beta$ -strands in opposite directions in parallel to the backbone axis (see Fig. 2a, inset). In this pulling setup, neighbouring strands were pulled in opposite directions, while no force was applied to the central strand in order to keep the symmetry in loading. Compared to similar studies,<sup>18,22</sup> this way of pulling involves both the axial and shear effects on the peptides in the crystal. Such a mechanical loading is closer to the situation in a fiber, where most of the strands are subjected to the forces of varying magnitudes depending on the connectivity between crystals.<sup>29</sup> The pulling setup described here is rather an idealized case that results in a homogeneous distribution of the pulling stress across the crystalline subunits, and therefore, can be expected to give an upper limit of the rupture stresses. The toughness of a crystalline subunit was calculated by integrating its stress–strain curve up to the rupture point at which the  $\beta$ -strands in the crystals disengage from each other.

## Finite Element (FE) simulations

FE simulations were performed for (i) the skeleton models of the crystalline subunits and (ii) the two-phase fiber model. All FE simulations were carried out with the COMSOL Multiphysics package. Nominal values of stress and strain were used in the calculations. We considered all systems as purely elastic, thereby neglecting the rate-dependent viscous and dissipative plastic effects.

The three-dimensional ‘skeleton model’ of the crystalline subunit was described previously.<sup>24</sup> In short, the skeleton models are built of isotropic Euler beams representing peptide

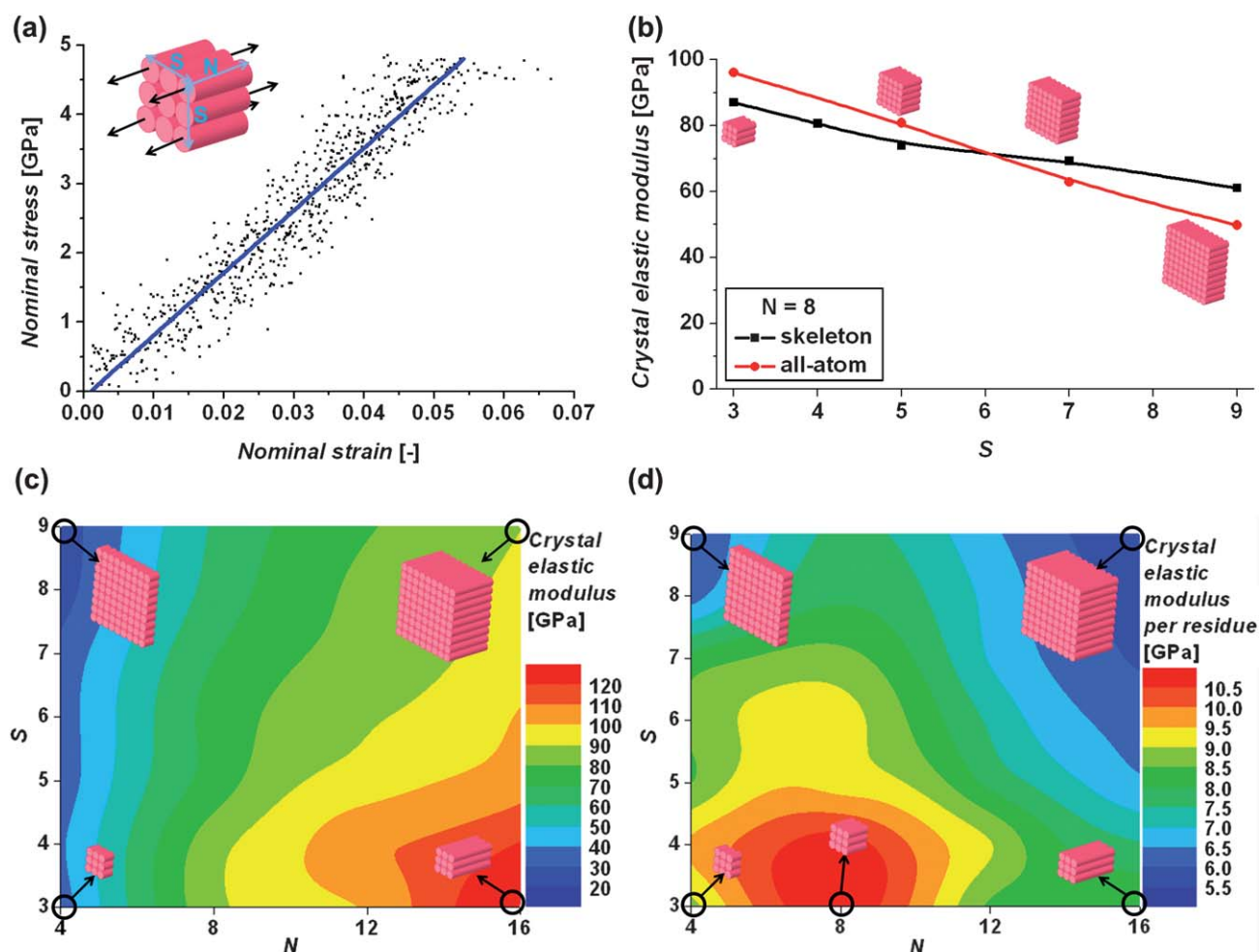


**Fig. 2** Mechanical properties of the crystalline subunits. (a) The stress–strain curve from the all-atom simulations of a crystalline subunit ( $N = 8$ ,  $S = 3$ ). Blue line shows a linear fit up to the rupture point. Inset shows the pulling setup. (b) A comparison of the all-atom and skeleton models showing the decrease in the axial elastic modulus with the number of layers,  $S$ . (c) A contour map constructed for the skeleton models showing the change in the axial elastic modulus with respect to  $N$  and  $S$ . (d) The normalized version of (c) showing the per residue contribution to the elastic modulus. Smooth lines in (b) are spline fits to the data points.

backbones and side-chain elements with linear elasticity, and hydrogen bonds with a strain dependent, non-linear elasticity. The starting geometry of the  $N = 8$ ,  $S = 5$  structure ( $\sim 2.7 \times 1.9 \times 2.0 \text{ nm}^3$ ), the nominal lengths of the included members and the elastic (Young's) moduli of these members were obtained from the equilibrium MD simulations performed with the corresponding all-atom model. For other crystal sizes, the skeleton models were built in proportion to the  $N = 8$ ,  $S = 5$  structure. The pulling setup for the skeleton models was the same as the one described for the all-atom models (Fig. 2a, inset).

The fiber model was a three dimensional solid stress–strain model composed of transversely isotropic crystalline subunits embedded into a matrix of isotropic amorphous subunits without any slip at the interfaces. The fiber was represented by a cylindrical solid member pulled by distributed loads acting on both ends. The fiber was 7 nm in radius and 39 nm in length. The crystalline subunits were randomly distributed in the fiber, but their longitudinal axes were kept aligned with the fiber axis.<sup>13</sup> Both types of subunits were treated as linear elastic solids. All fiber models were 25% crystalline by volume. The elastic modulus

of the amorphous subunit (2.7 GPa) was calculated from the all-atom model in our previous study.<sup>24</sup> For the crystalline subunits, the elastic moduli in axial and transverse directions and the shear moduli were calculated separately with the skeleton models of the corresponding geometries. Poisson's ratio for both types of subunits was assigned as  $\sim 0.33$  along the axial direction, as suggested by Fossey for poly(Gly-Ala) crystals.<sup>19</sup> Using the finite element scheme as implemented into COMSOL, the fiber was discretized into finite elements, for which, for a given external strain of the fiber, the internal stresses and strains were calculated. This requires to numerically solve the set of partial differential equations taking into account the stiffness matrices and boundary conditions. Here, we did not consider the yielding of the fiber, which allows for a further increase in the strain without the failure of the fiber. Therefore, the estimated rupture and toughness values present the lower limits of the actual values, respectively. Fiber rupture was assumed to happen at the instance where the average von Mises stress in the crystalline subunits reached their rupture stress in the corresponding all-atom models, which naturally depends on the crystal size.

The fiber toughness was calculated as half the product of the fiber rupture stress and strain.

## Results and discussion

Mechanical properties of artificial fibers could be tailored by controlling (i) the crystallinity level, (ii) the structural architecture (*e.g.* lamellar or random distribution), or (iii) the size of the subunits in the fiber. Recently, we have investigated the significance of the former two factors and confirmed that natural spider silks choose a moderate crystallinity level of 10–25% in order to achieve a balanced tradeoff between strength and elasticity.<sup>24</sup> Furthermore, distributions of crystalline subunits both in a random fashion or towards an ordered fashion in lamellae were found to be in agreement with experimental results. Considering the fiber toughness, lamellar distribution was found to be a more advantageous option for the structural architecture when designing artificial fibers with higher toughness. Here, we constrain the parameters regarding the fiber crystallinity and structural architecture (*i.e.* random distribution with 25% crystallinity), and investigate the size effects of the crystalline subunits by only varying the length of the  $\beta$ -strands,  $N$ , and the number of layers that build up a crystalline subunit,  $S$  (Fig. 1b).

### Mechanical properties of the crystalline subunits

Crystalline subunits mostly exhibited a linear stress–strain behavior as the  $\beta$ -strands were pulled in an alternating manner (Fig. 2a). We have observed a similar stress–strain profile also with other pulling setups (*e.g.* pulling a single strand out of a crystal, or pulling all  $\beta$ -strands from both termini).<sup>17,24</sup> Unlike the stick–slip mechanism of hydrogen bonds as suggested by Keten *et al.*<sup>18</sup> and Nova *et al.*,<sup>22</sup> the crystalline subunits in our all-atom simulations did not show such a plastic deformation prior to rupture. Such a discrepancy might arise from the boundary conditions applied on the crystalline subunit. In our simulations, the top and bottom layers of a crystalline subunit were not constrained. Therefore, the hydrogen bond network between the  $\beta$ -strands in the crystal did not lead to such a deformation regime.

Both the all-atom and skeleton models showed that the elastic modulus of the crystalline subunits decreases with increasing number of layers,  $S$  (Fig. 2b). Hence, a higher number of  $\beta$ -strands results in softer crystals. For instance, the all-atom models with  $S = 3$  and  $S = 9$  (with  $N = 8$ ) have elastic moduli of 96.0 GPa and 49.8 GPa, respectively. This observation qualitatively agrees with the one reported by Nova *et al.* although a different pulling setup was used.<sup>22</sup> The backbone length of the  $\beta$ -strands,  $N$ , on the other hand, has an opposite effect on the crystal elastic modulus (Fig. S1†). Our simulations showed that longer crystalline subunits from the skeleton and all-atom models have higher elastic modulus. The all-atom models with  $N = 4$  and  $N = 16$  (with  $S = 5$ ) had 19.8 GPa and 137.0 GPa elastic moduli, respectively. Despite their simplicity, the skeleton models quantitatively agree with the all-atom models and thus allowed us to investigate a larger set of values for  $N$  and  $S$  (Fig. 2b). Fig. 2c summarizes the effects of both geometrical parameters,  $S$  and  $N$ , on the crystal elastic modulus. It is clear that higher  $N$  and lower  $S$  values result in a higher elastic

modulus for the crystalline subunits. Longer  $\beta$ -strands with more intra-layer hydrogen bonds and smaller layers with less axial strain are the key determinants for a stiffer crystal, with a maximum elastic modulus of 134.6 GPa for  $N = 16$  and  $S = 3$ . However, if one considers the average contribution of each amino acid to the crystal stiffness, a different maximum emerges. As shown in Fig. 2d, we found a small cross-section ( $S = 3$ ) and an intermediate  $\beta$ -strand length ( $N = 8$ ) to be the mechanically optimal configuration, with each of its residues providing an average stiffness of 10.9 GPa.

Toughness is a measure of the required energy to rupture the crystals and can be inferred from the stress–strain profiles of the all-atom models in MD simulations. The toughness follows a trend similar to that observed for the crystal elastic modulus. The crystal toughness decreases with higher  $S$  (Fig. 3a) and increases with higher  $N$  values (Fig. 3b). For instance, the  $S = 5$ ,  $N = 8$  structure has 48.8 MJ m<sup>-3</sup> toughness, whereas the  $S = 7$ ,  $N = 8$  and  $S = 5$ ,  $N = 4$  structures have 35.4 and 26.5 MJ m<sup>-3</sup> toughness, respectively. Unlike the crystal elastic modulus, crystal toughness does not yield an optimum geometry in terms of the contribution per residue within the probed range of crystal size, but continues to increase (decrease) with  $N$  ( $S$ ). Considering the same crystal sizes, our toughness values overlap with the

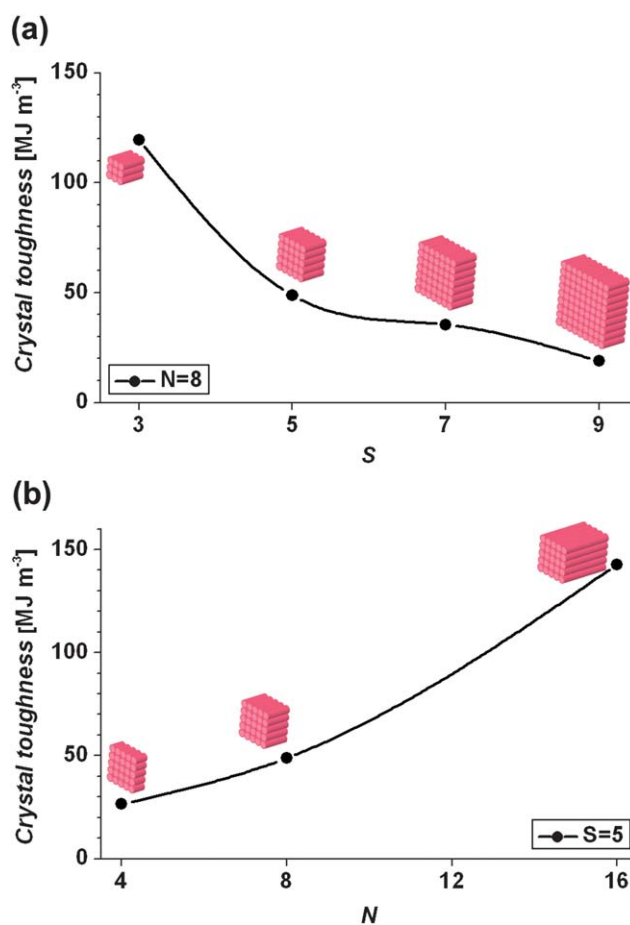


**Fig. 3** Toughness of the crystalline subunits. All-atom models show a decrease (a) and increase (b) with respect to the number of  $\beta$ -strands in the crystal,  $S$ , and the backbone length given by  $N$ , respectively. Smooth lines in (a) and (b) are spline fits to the data points.

resilience values reported by Keten *et al.*<sup>18</sup> By definition, resilience calculations consider only the elastic deformation region, while toughness involves the total energy input until the rupture point. In our simulations we have observed that the crystalline subunits showed little or no plastic deformation as suggested by a linear slope in the stress–strain curves (Fig. 2a). This suggests toughness and resilience to be highly similar for silk crystals, in contrast to the previous observations which, however, might be driven by boundary effects.<sup>18</sup>

The toughness and rupture properties of the crystalline subunits show size dependencies parallel to the crystal elastic modulus (also compare Fig. S2†). Taken together, they suggest that smaller  $S$  and larger  $N$  values yield stiffer and stronger crystals. In contrast to the previously suggested geometries,<sup>18,22</sup> we find that the crystals with lower aspect ratios, namely with several nm  $\beta$ -strand length and 1 nm<sup>2</sup> cross-sectional area, exhibit the highest mechanical performance. To the best of our knowledge, there have been no experimental studies to compare our findings, except from the observations that the crystal length along the fiber axis corresponds to 8–16 alanine residues.<sup>1,14</sup> Hence, we consider our results as valuable predictions to be tested by future experimental work. We anticipate, *e.g.*, a novel insight from measurements of both the fiber and crystal elastic moduli<sup>30</sup> for recombinant silk in which the length of the poly (alanine) sequence has been modified.

### Mechanical properties of the fibers

Crystalline subunits are one of the main constituents of natural silk fibers, but their contribution to the fiber mechanical properties cannot be straightforwardly predicted solely on the basis of the crystal mechanical properties. Here, we employ FE analysis to determine the fiber elasticity and toughness with respect to different crystal sizes. We limit our analysis by keeping the degree of ordering (25% crystallinity) and the structural architecture of the fiber (randomly distributed crystals) as fixed parameters. Although the total volume occupied by the crystalline subunits is

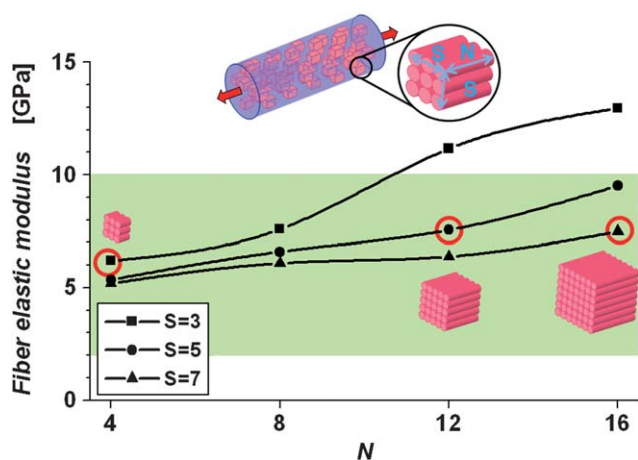


**Fig. 4** The variation of the fiber elastic modulus with respect to the crystalline subunit geometry obtained from FE calculations. Upper inset shows the pulling setup for the fiber and the green band indicates the range of experimental results in literature.<sup>1,4,5,8</sup> Representative crystal sizes are shown as schematics and highlighted by red circles. Smooth lines are spline fits to the data points.

the same in all fibers, the effect on the fiber elastic modulus changes with the crystal geometry. Fig. 4 shows that a smaller number of layers (*i.e.* smaller  $S$ ) yields stiffer fibers and this effect is more pronounced as  $N$  increases. As an example, fibers having crystals with  $S = 3$  and  $S = 7$  have similar elastic moduli at  $N = 4$  (6.2 GPa *vs* 5.2 GPa) while the difference is larger at  $N = 16$  (13.0 GPa *vs* 7.5 GPa). In a coarse-grained fiber model with a higher crystallinity rate (45%), Termonia has observed the same qualitative behavior for the fiber elastic modulus.<sup>21</sup> In an experimental study by Du *et al.*, spider silk fibers are reported to become stiffer with crystals having smaller  $S$  values, also supporting our observation.<sup>7</sup> In contrast to our finding, they reported that smaller  $N$  leads to stiffer fibers, which, however, can be ascribed to the higher crystallinity of their fibers with shorter crystals.

Our simulations with the all-atom and skeleton models showed that the elastic characteristics of the crystalline subunits resemble transversely isotropic materials. Consequently, the fiber model shows a transversely isotropic behavior. Contrary to the general assumption of isotropic crystals,<sup>9</sup> the crystalline subunits are stiffer in the axial direction and relatively weaker in the transverse directions while having low shear moduli. For instance, the skeleton model of the  $S = 5$ ,  $N = 8$  structure has axial, transverse, and shear moduli of  $\sim 74.0$ ,  $\sim 36.0$ , and  $\sim 6.2$  GPa, respectively. Fibers made of these crystals have 6.6 GPa axial tensile modulus, which falls well into the range of experimental values regarding spider silk (*Araneus diadematus*), 2–10 GPa.<sup>1,4,5,8</sup> Moreover, the compressive modulus of these fibers in the transverse direction, 0.7 GPa, agrees well with the experimental results for spider silk (*Nephila clavipes*), 0.6 GPa,<sup>11</sup> and silkworm silk (*Bombyx mori*), 0.7 GPa.<sup>31</sup>

We next assessed the second crucial parameter regarding mechanical performance; fiber rupture and the resulting fiber toughness. Despite the large number of experimental works addressing the toughness and rupture of natural silk fibers,<sup>1,4,5,8</sup> there is limited information regarding the size effects of the crystalline subunits. Although Du *et al.* reported the significance of the size effects on the silk fiber mechanics, they could not explicitly separate this effect from the contribution of variations in fiber crystallinity.<sup>7</sup> We here systematically investigated this size effect by varying the crystalline subunit size under constant crystallinity. Since our fiber model was based on conventional FE calculations, fiber rupture could not be directly simulated, but it was indirectly estimated from the failure of the crystalline subunits observed in the corresponding all-atom models (see Methods).

As the crystals within the fibers are composed of  $\beta$ -strands of increasing length  $N$ , the fiber toughness increases as much as an order of magnitude (Fig. 5a). A similar behavior was observed for the all-atom models of the bare crystalline subunits (Fig. 3b). On the other hand, the fibers with wider crystals (*i.e.* crystals with higher  $S$ ) tend to have lower toughness (Fig. 5b), again showing a similar trend as the bare crystalline subunits (Fig. 3a). However, the size dependency is less pronounced for the parameter  $S$ , the cross-sectional area. The overall increase in toughness with increasing  $N$  and decreasing  $S$  originates from two parallel tendencies, namely higher rupture strains and stresses (Fig. 5c and d). Overall, at moderate crystallinity, the highest fiber toughness is achieved with crystals composed of small layers of long  $\beta$ -strands. This observation is also valid for a serial (lamellar) arrangement of crystalline and amorphous

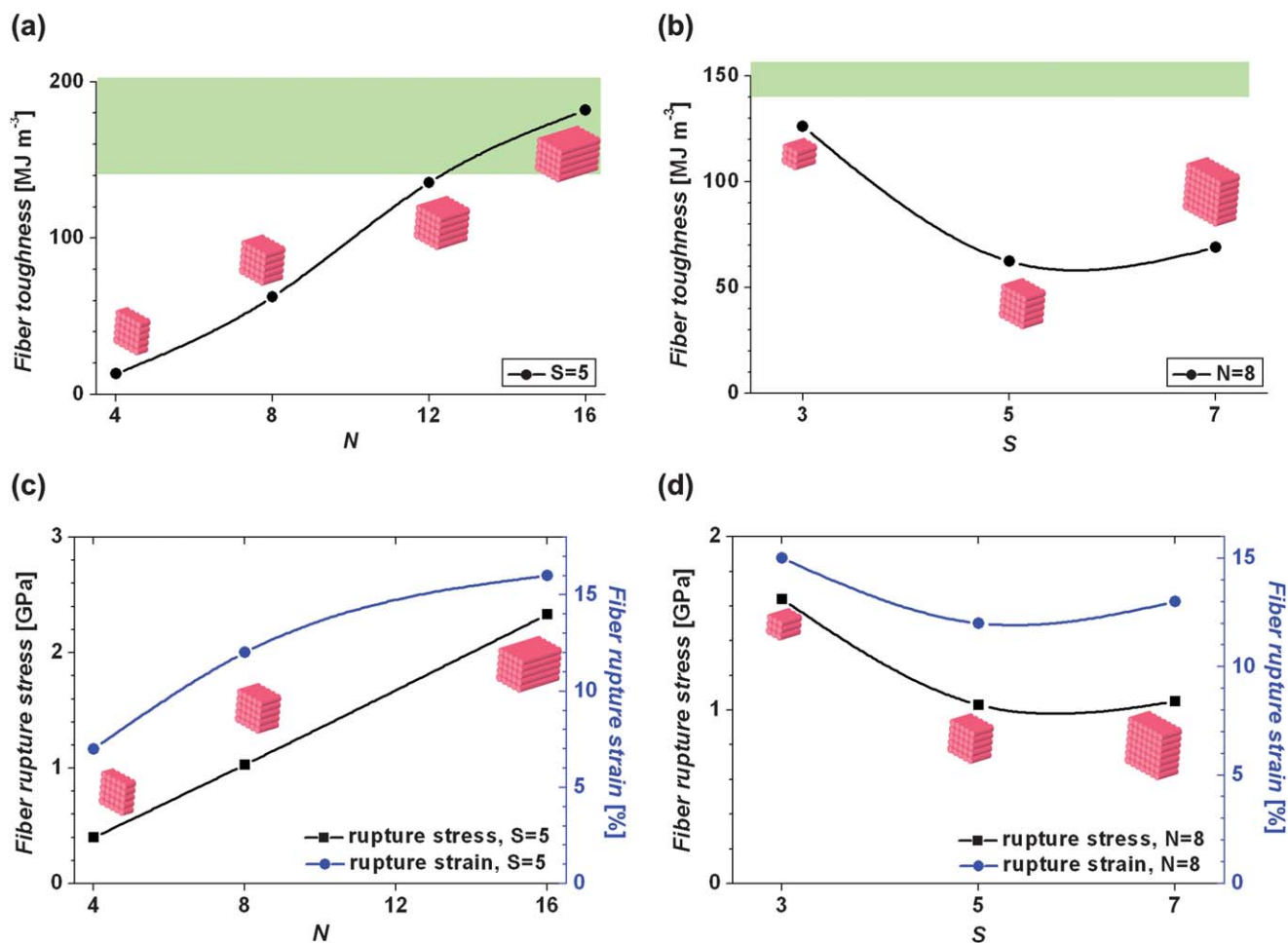


**Fig. 5** Fiber toughness and rupture properties obtained from FE calculations. (a–b) The variation of the fiber toughness with respect to the crystal size parameters,  $N$  (a) and  $S$  (b), is shown. Green bands in (a) and (b) indicate the range of experimental results in literature.<sup>1,4,5,8</sup> Fiber rupture stress and strain curves with respect to the crystal size parameters,  $N$  (c) and  $S$  (d). Smooth lines in (a–d) are spline fits to the data points.

subunits, but the toughness is of higher magnitude. For instance, fibers with  $N = 8$ ,  $S = 5$  crystals have a toughness of  $215.0 \text{ MJ m}^{-3}$  with a serial distribution of crystals, as compared to  $62.4 \text{ MJ m}^{-3}$  with the random arrangement conventionally assumed and considered in Fig. 5. In fact, we have already previously reported that a serial arrangement of subunits is superior over a random arrangement in terms of high fiber toughness.<sup>24</sup> As we now show here, nanometre-sized crystalline blocks of small cross-sectional area are the components of choice within these lamellae, the detailed arrangement of which on the molecular scale, however, is still open for discussion.

## Conclusions

Here, we have quantified the crystalline size effects on silk fiber mechanics with a bottom-up computational approach. A common conclusion is that crystalline and fiber mechanical properties show opposite trends with backbone length of the  $\beta$ -strands,  $N$ , and the number of the  $\beta$ -strand layers,  $S$ , in the crystals. In particular, elastic modulus, toughness, and rupture stress of crystalline subunits and fibers increase with  $N$  due to higher portions of forces carried by the backbone elements and hydrogen bonds across the backbones. On the other hand,

increasing  $S$  results in softer and weaker structures due to the predominant behavior of the more deformable side chain interactions between each  $\beta$ -strand layer in the crystal. Results from all-atom models of the crystalline subunits support this observation. All-atom models also show that the crystalline subunits do not undergo plastic deformations, but instead feature a purely elastic regime up to the rupture point.

FE simulations of the skeleton models of the crystalline subunits are in quantitative agreement with the all-atom models at a tremendously decreased computational cost. The skeleton models enable us to determine the mechanically optimal size for the crystalline subunits. Based on the elastic modulus calculations, the  $N = 8$ ,  $S = 3$  structure shows the most efficient usage of the protein crystalline material to maximize the crystal stiffness, in close agreement with the prevalence of roughly eight alanine residues in silk proteins and the experimentally determined crystal dimensions in silk fibers.<sup>1</sup> Our quantitative findings are based on poly(alanine) silk crystals, but the qualitative trends are expected to be observed also with poly(GA) crystals due to their similar structural architectures.

In order to determine the contribution of the crystalline subunits on fiber mechanical properties, FE simulations of the comprehensive fiber model allow us to reach mesoscopic length

scales at a feasible computational cost. Being composed of transversely isotropic crystal blocks, the simulated silk fibers show a similar material behavior. The calculated tensile and transverse elastic moduli are in good agreement with the experimental results in literature. The fiber stiffness is found to be strongly dependent on the crystalline subunit stiffness when  $S = 3$ , and this effect is less pronounced for larger cross-sections. The fiber toughness substantially increases with the length of the strands in the crystal, but again is largely unaffected for higher number of layers (*i.e.*  $S > 3$ ). In contrast to previous studies, other fiber parameters such as fiber crystallinity and structural architecture are constrained, allowing us to systematically scan silk fiber mechanics as a function of crystalline subunit dimensions. Given the challenge to experimentally determine the crystalline subunit dimensions, our study provides a guide for artificial fiber design.

Our results on fiber toughness are based on two major approximations. First, the fiber rupture stress is directly estimated from the crystal rupture stress so that the plastic deformations in the fiber following crystal rupture are neglected. Secondly, the non-linear elasticity of the amorphous subunit is approximated by a linear model. Therefore, the toughness values provided here have to be considered as the lower bounds of the results to be expected in the experiments (Fig. 5a and b). Important future steps include the plastic deformation in the fiber, more specifically in the amorphous phase, and employing a more detailed model for the amorphous subunit that takes connectivity and non-linearity into account. Despite the drawbacks mentioned above, the FE models allow us to sample a large set of design possibilities with acceptable accuracy and affordable computational cost. Our computational approach combining MD simulations and FE analysis does not make use of any empirical parameters and is easily applicable to similar semicrystalline systems such as non-biological block copolymers or composite systems.

## Acknowledgements

This study was supported by a postdoctoral fellowship of the Alexander von Humboldt Foundation (to M.C.), the Klaus Tschira Foundation, the Chinese Academy of Sciences, and the Global Networks program at Heidelberg University as part of the Excellence Initiative.

## Notes and references

- 1 J. M. Gosline, P. A. Guerette, C. S. Ortlepp and K. N. Savage, *J. Exp. Biol.*, 1999, **202**, 3295.
- 2 C. Vepari and D. L. Kaplan, *Prog. Polym. Sci.*, 2007, **32**, 991.
- 3 K. N. Savage and J. M. Gosline, *J. Exp. Biol.*, 2008, **211**, 1937.
- 4 Y. Liu, A. Sponner, D. Porter and F. Vollrath, *Biomacromolecules*, 2008, **9**, 116.
- 5 B. O. Swanson, T. A. Blackledge, J. Beltran and C. Y. Hayashi, *Appl. Phys. A: Mater. Sci. Process.*, 2006, **82**, 213.
- 6 S. Rammensee, U. Slotta, T. Scheibel and A. R. Bausch, *Proc. Natl. Acad. Sci. U. S. A.*, 2008, **105**, 6590.
- 7 N. Du, X. Y. Liu, J. Narayanan, L. Li, M. L. M. Lim and D. Li, *Biophys. J.*, 2006, **91**, 4528.
- 8 T. Koehler and F. Vollrath, *J. Exp. Zool.*, 1995, **271**, 1.
- 9 R. Ene, P. Papadopoulos and F. Kremer, *Soft Matter*, 2009, **5**, 4568.
- 10 N. Becker, E. Oroudjev, S. Mutz, J. P. Cleveland, P. K. Hansma, C. Y. Hayashi, D. E. Makarov and H. G. Hansma, *Nature.*, 2003, **2**, 278.
- 11 F. K. Ko and J. Jovicic, *Biomacromolecules*, 2004, **5**, 780.
- 12 F. Hagn, L. Eisoldt, J. G. Hardy, C. Vendrely, M. Coles, T. Scheibel and H. Kessler, *Nature*, 2010, **465**, 239.
- 13 J. D. van Beek, S. Hess, F. Vollrath and B. H. Meier, *Proc. Natl. Acad. Sci. U. S. A.*, 2002, **99**, 10266.
- 14 D. T. Grubb and L. W. Jelinski, *Macromolecules*, 1997, **30**, 2860.
- 15 T. Asakura, M. Okonogi, Y. Nakazawa and K. Yamauchi, *J. Am. Chem. Soc.*, 2006, **128**, 6231.
- 16 H. Shulha, C. W. P. Foo, D. L. Kaplan and V. V. Tsukruk, *Polymer*, 2006, **47**, 5821.
- 17 S. Xiao, W. Stacklies, M. Cetinkaya, B. Markert and F. Gräter, *Biophys. J.*, 2009, **96**, 3997.
- 18 S. Keten, Z. Xu, B. Ihle and M. J. Buehler, *Nat. Mater.*, 2010, **9**, 359.
- 19 S. A. Fossey and S. Tripathy, *Int. J. Biol. Macromol.*, 1999, **24**, 119.
- 20 Y. Aoyanagi and K. Okumura, *Phys. Rev. Lett.*, 2010, **104**, 038102.
- 21 Y. Termonia, *Macromolecules*, 1994, **27**, 7378.
- 22 A. Nova, S. Keten, N. M. Pugno, A. Redaelli and M. J. Buehler, *Nano Lett.*, 2010, **10**, 2626.
- 23 S. Xiao, W. Stacklies, C. Debes and F. Gräter, *Soft Matter*, 2011, **7**, 1308.
- 24 M. Cetinkaya, S. Xiao, B. Markert, W. Stacklies and F. Gräter, *Biophys. J.*, 2011, **100**, 1298–1305.
- 25 D. van der Spoel, E. Lindahl, B. Hess, G. Groenhof, A. E. Mark and H. J. C. Berendsen, *J. Comput. Chem.*, 2005, **26**, 1701.
- 26 W. L. Jorgensen and J. Tirado-Rives, *J. Am. Chem. Soc.*, 1988, **110**, 1657.
- 27 W. L. Jorgensen, J. Chandrasekhar, J. D. Madura, R. W. Impey and M. L. Klein, *J. Chem. Phys.*, 1983, **79**, 926.
- 28 T. Darden, D. York and L. Pedersen, *J. Chem. Phys.*, 1993, **98**, 10089.
- 29 M. Cetinkaya, S. Xiao and F. Gräter, *Phys. Chem. Chem. Phys.*, 2011, **13**, 10426.
- 30 I. Krasnov, I. Diddens, N. Hauptmann, G. Helms, M. Ogurreck, T. Seydel, S. S. Funari and M. Müller, *Phys. Rev. Lett.*, 2008, **100**, 048104.
- 31 K. Zhang, F. W. Si, H. L. Duan and J. Wang, *Acta Biomater.*, 2010, **6**, 2165.